Published in Materials & Design, July, 2016
doi: 10.1016/j.matdes.2016.07.035

An Experimental Investigation into Multi-Functional Z-pinned Composite Laminates

B. Zhang[a,*], G. Allegri[b], S.R. Hallett[a]

[a]Advanced Composites Centre for Innovation and Science (ACCIS),

University of Bristol, Queen's Building, University Walk, Bristol BS8 1TR, UK

[b] Department of Aeronautics, Imperial College London,

South Kensington Campus, London SW7 2AZ, UK

Abstract

This paper investigates the feasibility of monitoring progressive delamination growth in Z-pinned composite laminates via the measurement of through-thickness electrical resistance. This novel health monitoring technique is based on connecting Z-pins both in series and in parallel by means of arrays of electrodes arranged on the laminate surfaces. This creates a multi-functional (through-thickness reinforcing and sensing) laminated structure. Experimental results on double-cantilever beam coupons demonstrate that the entire Mode I bridging response of Z-pins can be monitored, from the arrival of the delamination front to the complete pull-out of the through-thickness reinforcement. Hence the extent of delamination can be inferred from the through-thickness resistance. This is proved for both conductive (carbon fibre-reinforced) and non-conductive (glass fibre-reinforced) laminates. The premature Z-pin failure during progressive pull-out corresponds to an abrupt increase of through-thickness electrical resistance. The delamination sensing/suppression method presented in this paper can be readily applied to Z-pinned composites at structural level.

Keywords: Structural composites; Z-pins; Delamination; Fracture toughness; Health monitoring.

*Corresponding author: b.zhang@bristol.ac.uk (B. Zhang); +44(0) 117 33 15311

Published in Materials & Design, July, 2016
doi: 10.1016/j.matdes.2016.07.035

1. Introduction

1.1 State of the art

Fibre-reinforced plastics (FRP) composites today find a wide range of engineering applications due to their excellent in-plane specific stiffness and strength. The all-electric car BMW i3 features a carbon FRP passenger compartment [1]. The Airbus A350-XWB and Boeing B787 airframes contain 53% and 50% FRP composites, respectively [2]. However, FRP composites are prone to delamination, i.e. the progressive through-thickness dis-bond of individual plies assembled in laminate stacks. Delamination may be caused by inherent features that act as interlaminar stress risers in composite laminates, such as free edges and ply drop-offs. The susceptibility of FRP to delamination is particularly significant under impact loading. Aiming to improve the delamination resistance of laminated composites, the past decades have seen the advance of several through-thickness reinforcement (TTR) techniques, such as stitching [3], tufting [4], braiding [5] and 3D weaving [6].

Z-pinning is an effective TTR method, whereby individual metal or composite rods are inserted through the laminate thickness before [7], during[8] and after [9] cure. In the literature, the methodologies for the experimental characterisation and modelling of delamination suppression in Z-pinned laminates follow a multi-level/multi-scale overarching philosophy. This progresses from the characterisation and modelling of single Z-pin behaviour to the prediction of delamination suppression provided by arrays of Z-pins bridging interfaces, which is validated by means of experimental data at coupon and structural element levels. Mode I tests on single Z-pin coupons show that the bridging action becomes more effective for longer insertion length [10], since the energy dissipation associated with friction pull-out increases. However, there exists a critical insertion length that must not be exceeded, otherwise the frictional forces would cause the premature failure of the Z-pin, with a consequent drop in apparent fracture toughness [11]. Regarding Mode

II behaviour, the experimental evidence proves that composite Z-pins tend to fail in shear without experiencing significant pull-out [12]. On the other hand, metal Z-pin can experience a substantial amount of shear deformation, thus providing an effective toughening action. Generally speaking, the Z-pin response varies from complete pull-out to fracture as the mode-mixity ranges from pure Mode I to pure mode II [13]; hence, in principle, the bridging performance can be tailored by varying the Z-pin insertion angle [14], albeit some amount of "misalignment" is always present due to manufacturing variability.

Several models have been proposed to predict the behaviour of single Z-pins. These include: 1) semi-analytical approaches based on shear lag assumptions [15], eventually coupled with elementary beam theory [16,17]; 2) "high-fidelity" finite element analysis (FEA) at single Z-pin level [18,19]. These two kinds of approaches are complementary, rather than mutually exclusive. High-fidelity FEA at single Z-pin level is computationally expensive, so semi-analytical approaches, once properly calibrated, provide a means of "reduced order modelling" that eases the transition among scales.

ASTM/ISO standard coupons comprising Z-pin arrays inserted along the delamination path are usually employed to evaluate the toughening enhancement due to the presence of the TTR elements in Mode I/II [20,21] and mixed-mode (MMB) regimes [22]. The apparent interlaminar fracture toughness of Z-pinned composites is much larger than for un-pinned laminates over the full mode-mixity range. This enhancement increases with the Z-pinning areal density, although the corresponding in-plane stiffness and strength properties are degraded. At element level, the effectiveness of Z-pins in delaying/preventing dis-bonds had been assessed on Tee- [23], lap- [24] and L-joints[25]. Z-pins in structural elements increase both the delamination initiation and the ultimate failure loads, allowing a more progressive growth of interlaminar cracks and a substantial improvement of the work to failure. Regarding impact behaviour, Z-pinning significantly reduces the post-impact delamination area. This favourable effect is further promoted in relatively thick laminates

[26]. The reduction of delamination area also causes a significant increase of compression after impact strength of Z-pinned laminates [27].

Numerical models have also been established to investigate the fracture mechanics of Z-pin array reinforced composites. Early FEA approaches have been based on the virtual crack closure technique [24], with nonlinear spring elements distributed on the delamination surfaces to model the bridging action of Z-pins. More recent techniques are based on the formulation of cohesive zone models whereby the response of individual Z-pins is homogenised at interface level [28,29]. The interface cohesive constitutive behaviour is based on traction-displacement laws derived from single Z-pin experiments or models.

1.2 Beyond the state of the art

The majority of the existing research on Z-pinning is focussed on the delamination arrest function of Z-pins, and, as a consequence, on the mechanical performance of Z-pinned laminates. On the other hand, it has been demonstrated that un-pinned conductive (carbon fibre reinforced) laminates have a strain/damage self-sensing capability, which can be exploited via electrical resistance (ER) or electric potential measurements [30–32]. It is worth stressing that "self-sensing" is here intended as the inherent capability of a laminate to generate a detectable change in electrical signal whenever damage occurs, without the need for additional sensing elements. As will be demonstrated later, the presence of conductive TTR elements enhances the inherent self-sensing ability of conductive laminates. A Z-pin can be in principle made of any material that can be processed into small diameter rods. This means that electrically conductive Z-pins may also endow a non-conductive laminate with a delamination sensing function, as it will be shown in this paper.

This paper first introduces a novel concept of multi-functional through-thickness reinforced composite laminates, whereby Z-pins enable both delamination sensing and through-thickness reinforcement. This concept is then demonstrated at coupon level by

means of double-cantilever beam (DCB) carbon-fibre and glass-fibre specimens, both reinforced with carbon-fibre Z-pins.

2. Multi-functional method

The intrinsic ability of single Z-pin reinforced laminate to sense delamination through a change in the through-thickness electrical resistance (TTER) has been demonstrated in [33]. This approach is here further developed and scaled up to coupon level, considering DCB laminated specimens comprising arrays of embedded Z-pins. The multi-functional method for delamination sensing/mitigation proposed here is based on having the Z-pins in the laminate protruding from the top and bottom surfaces with arrays of electrodes attached to the Z-pin ends. Since the Z-pins act as sensing elements for the TTER of the composite, the Z-pinned laminate can be considered as a self-sensing structure, whose multi-functionality (mechanical and sensing) is enabled by the Z-pins. The self-sensing laminate in general comprises multiple TTER measurement channels. These consist of surface electrodes and through-thickness Z-pins, which can be in principle connected to the electrodes in various series/parallel configurations. The electrodes of a sensing channel can be classified into: 1) terminal electrodes used for the electrical connection between Z-pins and signal acquisition devices; 2) intermediate electrodes employed only for the electrical connection between Z-pins. These definitions are here applied in a loose sense, since a terminal electrode may also be used for the electrical connection between Z-pins. As mentioned above, in the sensing configurations considered here, the electrodes are attached directly onto the laminate surfaces, with no insulating media in between.

3. Experimental Method

In order to verify the feasibility of the multi-functional approach to delamination sensing and mitigation, Z-pinned DCB coupons were manufactured and tested. Commercial T300/BMI Z-pins with the diameter of 0.28 mm were employed.

3.1 Specimen manufacture

Published in Materials & Design, July, 2016
doi: 10.1016/j.matdes.2016.07.035

The configuration and dimensions of a DCB coupon are shown in Fig. 1, based on the ASTM D5528 standard [34]. The coupons were made of 48 plies of unidirectional prepreg, with a quasi-isotropic (QI) stacking sequence: $[[0/90/-45/45]_{3s}]_s$. Strictly speaking, the ASTM standard applies only to the fracture toughness characterisation of unidirectional stacks. A QI stacking sequence has been considered here since it is more representative of structural laminate configurations. A PTFE film is inserted at the laminate mid-plane, between zero direction plies, to simulate the presence of a delamination, which is progressively grown from the insert under quasi-static loading. In order to evaluate the effect of the electrical conductivity of laminates on the delamination detection, two different pre-preg materials were employed, namely: conductive IM7/8552 (carbon/toughened-epoxy) pre-preg and non-conductive E-glass/913 (glass/epoxy) pre-preg. Both pre-pregs were supplied by Hexcel, UK. The initial delamination length was 25 mm for both the sets of coupons. A 20 mm long region from the tip of the PTFE insert was left un-pinned. As shown in Fig. 1, an array of 16 × 5 (row × column) Z-pins (areal density of 0.5%) was longitudinally inserted ahead of the un-pinned region. Each of the Z-pins protruded 1 mm from the top and bottom surfaces of the coupon. 16 silver/epoxy (1:1 weight ratio) electrode strips were bonded to both surfaces of the coupons. Each electrode was connected to a single row of Z-pins on each side, as shown in Fig. 1. Thus, each DCB coupon comprised 16 TTER sensing channels in total. Each channel consisted of one top electrode, one bottom electrode and one row of Z-pins. The Z-pins in a sensing channel were connected to the two surface electrodes as resistors in parallel. The TTER between the two electrodes in each channel was measured as a sensing variable by connecting the electrodes to a data acquisition system, which is described in the next subsection.

Due to the electrode arrangement, the Z-pinned coupons required a different manufacture process in comparison with the “mechanical” Z-pin specimens described in [13]. Specifically, a laminate was first assembled laying-up 48 plies and de-bulking under

vacuum pressure, with the PTFE film (artificial delamination) inserted at the mid-plane constituting the starter crack. Rubber sheets 1 mm thick were placed on the top and bottom surfaces of the laminated plate. The Z-pins were inserted through the entire thickness of the laminate/rubber sheets assembly. The excess Z-pin lengths were sheared off on both sides of the rubber sheets. The whole plate was packaged in a vacuum bag and then autoclave cured. The rubber sheets were peeled off once the laminate had been cured, leaving 1 mm long Z-pin ends protruding from the bottom and top surfaces of the laminate. The plate was then carefully cut into individual coupons and hinges were bonded to the coupons using AS89.1/AW89.1 adhesive (Cristex Ltd, UK). Next, the surfaces of the coupon were cleaned using acetone, before bonding the electrodes. The latter were placed on the coupon surfaces with the aid of removable moulds. Each mould had a central slot to accommodate the rows of protruding Z-pin ends and the electrodes. Lateral slots in the moulds helped to connect conductive wires to the electrodes. A silver-loaded epoxy adhesive was brushed into the moulds. The specimens with the un-cured electrodes were placed into an oven for curing at 80 °C for 15 minutes, and then gradually cooled down. The final coupons with individual electrode pairs and connecting wires were finished by removing the moulds and milling off any excess silver-loaded epoxy between adjacent electrodes.

3.2 Testing set-up

Mechanical loading was applied to the DCB using an Instron 8872 servo-hydraulic machine, equipped with a 1 kN load cell. A snapshot of a DCB coupon in the testing rig is shown in Fig. 2. The applied opening displacement rate was 2 mm/min. A paper ruler strip with a 1 mm scale was attached on one lateral edge of the sample for recording the crack length via a video camera. Since each TTER measurement channel comprises a single Z-pin row, the words “channel” and “row” will be considered as synonyms in what follows.

The data acquisition system consisted of: 1) a Keithley 2700 digital multimeter (DMM) as the ER measurement unit; 2) a Keithley 7703 multiplexer as the channel selection unit; 3)

a PC running NI/LabVIEW to record and synchronise load/displacement/ER data. The ER in all the sensing channels was measured in a sequential fashion. The ER resolution and sampling rate for each channel were set respectively to 6.5 digits and 3 readings/s. The data acquisition system also comprised: 4) an RS232-USB module for the data transmission between the PC and the DMM; 5) a PCI-9114 data acquisition card for the data transmission between the PC and the servo-hydraulic machine.

4. Experimental Results

4.1 Z-pinned carbon-fibre DCB coupons: mechanical response

A representative force vs. opening displacement curve for the carbon-fibre reinforced polymer (CFRP) coupons is presented in Fig. 3a. Initially, the response of the DCB coupon was elastic and the load increased linearly. The onset of delamination propagation occurred with a sudden load drop, which was followed by a further monotonic decrease, until the interlaminar crack reached the first Z-pin row. When the delamination grew into the Z-pinned area, the load again increased. A Z-pin bridging region progressively developed in the wake of the delamination tip, until the first TTR row experienced complete pull-out. During the development stage of the bridging region, the load increased because the number of Z-pins experiencing progressive pull-out progressively became larger. When the pull-out of the first Z-pin row was complete, the delamination tip was located between the ninth and tenth TTR rows. This also marked the onset of a "steady-state" bridging regime, whereby the bridging region was fully developed and it translated in an almost self-similar fashion with the crack tip. This happened because, as soon as a Z-pin row had been fully pulled out in the crack wake, the delamination front impinged one more TTR row. Since the distance between Z-pin rows was 3.5 mm, the length of the fully developed bridging region was approximately 30 mm, also corresponding to a total delamination length of approximately 75 mm. A maximum load of 325 N was recorded just before a steady-state bridging regime was reached. In the steady-state regime the opening force displayed an overall decreasing

trend. As the delamination front crossed the last Z-pin row, the delamination propagation quickly accelerated, since the bridging region started to become shorter. The load dropped at a much faster rate and all the DCB coupons quickly experienced full delamination.

Video recording showed that the Z-pins in channels 11 to 16 were suddenly pulled out due to the final catastrophic delamination propagation. On the other hand, the Z-pins in channels 1 to 10 had been completely pulled out before the sudden dis-bond. This implies that the Z-pins in channels 1 to 10 experienced their whole pull-out process at a constant displacement rate controlled by the loading machine, while the pull-out of the last six rows of Z-pins took place in an unstable fashion and at a much higher rate. However, post-mortem observations in Fig. 3b show that no Z-pin in the coupon failed, even in the last six rows.

4.2 Z-pinned carbon-fibre DCB coupons: sensing response

Regarding the delamination self-sensing performance of the CFRP coupon, the fractional ER change vs. time relationships for all the 16 channels are given by the blue curves in Fig. 4. The delamination arrival time at the nominal centre of a Z-pin row is indicated by a dashed red line, while the dashed black line represents the time at which complete pull-out occurred. Both the delamination arrival and full pull-out times were measured from video recordings of the tests. Note that the interlaminar crack may impinge an individual Z-pin earlier or later with respect to the nominal geometrical centreline of the row that the Z-pin belonged to. This is unavoidable, since Z-pins are always slightly misaligned, both in plane and through the thickness. Moreover, in a DCB specimen, the actual delamination front is never perfectly straight across the width [35].

The TTER signals exhibited consistent trends for each channel in the CFRP coupons. Until delamination arrival, the channel TTER did not vary. The initial TTER value ranged between 17 Ω and 75 Ω, depending on the channel considered. As the interlaminar crack approached the channel, the ER signal increased in some cases, e.g. channels 3, 7, 12 and

16 in Fig. 4. The mechanisms causing the TTER to increase are: 1) the Z-pin elongation, increasing the Z-pin ER; 2) the reduction of the Z-pin/electrode contact area, caused by the cross-sectional contraction of the Z-pin due to the Poisson effect and progressive failure of the Z-pin/electrode interface – all these mechanisms increase the Z-pin/electrode contact ER; 3) the reduction of the Z-pin/laminate contact area, which is also a result of the cross-sectional pin contraction and that raises the Z-pin/laminate contact ER. The effect of the Z-pin extension on the TTER is minor compared with other two mechanisms. A detailed analysis on these mechanisms can be found in bridging tests of single Z-pin reinforced coupons [33]. On the other hand, each of the channels experienced a rapid TTER decrease when the delamination fully impinged the corresponding TTR row. Three more mechanisms dictate this behaviour, namely:

4) The bending of the DCB arms increases the contact pressure between Z-pins and electrodes, this it decreases the Z-pin/electrode contact ER the overall channel TTER. This is qualitatively illustrated in Fig. 5a, where the crack is shown to approach a Z-pin. The opening shear forces behind the crack tip (left) are balanced by closing shear forces ahead of the delamination front (right), which cause interlaminar compression ahead of the crack tip. Surface longitudinal stresses due to bending are compressive for both the bottom and top surfaces. These stresses “squeeze” the electrodes around the Z-pin tips, reducing the local contact ER as mentioned above;

5) As the delamination advances within a row, the Z-pins de-bond first from the electrodes. Hence, the applied axial stress drops and the TTR axial elastic elongation is reduced, thus decreasing the channel TTER;

6) When the axial elongation is reduced, the Z-pin also swells radially, due to Poisson’s effect, and this also decreases the Z-pin/electrode and Z-pin/laminate contact ERs. Overall, there is also some variability in the magnitude of the actual TTER drop with respect to the delamination arrival time, but the associated trend is consistent for all the channels.

When the crack front reached a position just ahead of a given channel, the Z-pins started to be pulled out first from one of the surface electrodes (either bottom or top), as illustrated in Fig. 5b. This is consistent with experimental observations in the literature, where it has been reported that Z-pin pull-out always occurs in an asymmetric fashion [13], i.e. from only one of the split sub-laminates (DCB arms). Asymmetric pull-out can be clearly appreciated in the post-failure image of a DCB coupon shown in Fig. 3b. At the early stages of Z-pin pull-out, the TTER signal either reached a plateau, as seen in channels 1, 7 and 10, or it continued decreasing, but at a smaller rate, as for channels 3, 4, 5 and 14. This stage of the overall electro-mechanical response will be from now on denoted as "pull-out from electrode" (POFE).

Eventually, as the delamination progressed, the pull-out displacement would become large enough for the Z-pin to slide completely out of one of the surface electrodes, causing a rapid increase of TTER. After all the Z-pins in a channel were pulled out from one of the electrodes, the TTER continued steadily to increase; at this stage the Z-pins were sliding within the laminate, as shown in Fig. 5c. However, the overall electrical circuit for each channel was still closed because the laminate was conductive. This regime of the overall electro-mechanical response will be from now on indicated as "pull-out from laminate" (POFL).

Even when the pull-out of all the Z-pins in a row was complete, the TTER of the corresponding channel still had a finite value due to the conductivity of the laminate. The TTER values in all the channels diverged once the two halves of the DCB coupons were fully dis-bonded, i.e. at the end of the test. The TTER results show that when the crack started propagating in an unstable fashion, channels 11 to 14 were in the POFL stage, while the channels 15 and 16 were still in the POFE regime.

4.3 Z-pinned glass-fibre DCB coupon: mechanical response

A representative load vs. opening displacement curve for the glass-fibre reinforced

polymer (GFRP) coupons is presented in Fig. 6a. Overall, GFRP DCBs showed a mechanical response qualitatively similar to that of CFRP coupons. The two Z-pin bridging stages (bridging-developing and steady-state) are indicated in Fig. 6a. The GFRP coupons offered lower fracture resistance in the un-pinned region compared to CFRP DCBs. This is not surprising, since the 913 epoxy matrix has lower mode I fracture toughness than the 8552 system. However, a higher fracture resistance was observed in the GFRP coupons as soon as the delamination front entered the Z-pinned region. This is because carbon-fibre Z-pins require larger pull-out forces in GFRPs than in CFRPs, as found in single Z-pin bridging tests [33]. For the same reason, some Z-pins in the GFRP coupons failed by fibre fracture during the steady-state Z-pin bridging stage. Post-mortem observations (Fig. 6b) show one broken Z-pin in row 5, one in row 7 and two in row 8. The pin rupture was accompanied by two crack jumps, which correspond to the two load drops in Fig. 6a. Most interestingly, the failure of the Z-pins can be clearly identified from the TTER measurements that will be presented in the next section. In addition, video recording shows that the Z-pins in rows 3 and 4 were simultaneously pulled out at a high rate due to the first crack jump. The Z-pins in rows 11 to 16 were suddenly and completely pulled out due to the final catastrophic DCB dis-bond. One of the Z-pins failed in row 13, while all the others were fully pulled out.

4.4 Z-pinned glass-fibre DCB coupon: sensing response

The relative TTER change vs. time relationships for all the 16 channels in a GFRP coupon are presented in Fig. 7. The initial TTER values for the individual channels ranged between 35 Ω and 180 Ω. The channel TTER in the GFRP coupons may in some cases increase just before the delamination arrival, as seen in the zoomed plots in Fig. 7. After a channel had been reached by the crack front, the TTER value consistently decreased. This is again due to the same mechanisms as explained in Section 4.2 for carbon-fibre DCB coupons. When the Z-pins in a channel started to be pulled out from the electrodes, the

TTER signal tended to reach a plateau, as shown by the majority of the channel recordings in Fig. 7. With further loading, the full Z-pin pull-out from one of the electrodes was accompanied by an overall TTER increase, either with a continuous rapid trend or in a step-like form. This behaviour is consistent with what observed in CFRP coupons. However, a finite TTER value was observed even when the Z-pins were sliding into the laminate, despite the fact that GFRP is not conductive. This is because some carbon fibres originally belonging to the Z-pins remained attached to the surface of the pull-out channel [33]. These fibres maintained the electrical connection between the electrodes and the Z-pins. The presence of these fibres has been confirmed by microscopic observations in [33]. However, the resulting TTER variation was characterised by a noise level much larger than in the case of the conductive CFRP coupon in the POFL regime. Overall, the TTER signal allowed detecting the full pull-out process of the Z-pins in each channel, as well as the associated progressive delamination of the coupon. Suddenly diverging TTERs mark the final catastrophic dis-bond of the DCB coupons (open circuits for all channels). In addition, the abrupt TTER increases in channels 5 and 7 at 565 seconds indicated that the first crack jump was accompanied by rupture of Z-pins in both channels. Failure of a Z-pin implies that a resistor disappears in the channel 5-pin parallel circuit, thus the TTER increases according to classical parallel-resistor principle. For the same reason, rupture of Z-pins in channel 8 at 648 seconds can be identified from the TTER measurements as being simultaneous with the second crack jump.

5. Discussion

The differences in TTER values between the CFRP and GFRP coupons are due to non-conductive nature of the latter. In the CFRP coupons, part of the applied channel current flows through the DCB arms and also through Z-pins belonging to other rows. In the GFRP coupons, all the injected current must flow through the Z-pins in the corresponding channel. Nevertheless, considering the overall remarkable similarity between

the TTER trends for the two materials, it is evident that the Z-pins control the channel TTER, as long as they are not fully pulled out from the electrodes. The conductivity of CFRP coupons leads to a less noisy TTER signal in the POFL regime.

Regarding the mechanical performance of the Z-pinned laminates, the mode I baseline fracture toughness in the unpinned regions was about 0.3 kJ/m^2 for CFRP and 0.2 kJ/m^2 for GFRP. In the steady-state bridging regime, the material apparent fracture toughness was 8 kJ/m^2 and 10 kJ/m^2 respectively for CFRP and GRFP. Hence, a 0.5% areal density of Z-pins is sufficient to increase the fracture toughness by at least one order of magnitude with respect to the unpinned baselines. Therefore, the Z-pins can be considered as sensors that also enhance the fracture performance, which makes their application particularly advantageous. On the other hand, it is well known that Z-pinning reduces the in-plane stiffness and strength of composite laminates. The severity of the stiffness/strength knockdowns increases with the Z-pin areal density and diameter. However, the experimental data presented in [36] suggest that the in-plane knockdowns of mechanical properties can be estimated at a few percentage point for an areal density of 0.5% and 0.28 mm Z-pin diameter, as considered in this study. These knockdowns can most likely be tolerated, given the substantial increase in toughness and the delamination sensing function that the Z-pins enable. The weight increase due to the presence of the surface electrodes is around 10% compared to “mechanical” DCB coupons. This is clearly a potential limiting factor for practical applications of the sensing method described here. However, much thinner electrodes (e.g. tens of μm thick) could be 3D-printed on the laminate surface in order to mitigate the mass penalty. Moreover, for the sensing method to work in conductive laminates it is not necessary to have the Z-pin ends inside the electrodes. Indeed, the TTER variation in the POFL regime is sufficient to determine the location of the delamination front.

Finally, multi-physics FE modelling of unpinned delaminated plates [37] suggests that

the presence of delamination causes a through-thickness resistance change in the order of 1%. For Z-pinned laminates, the variation of through-thickness conductivity is at least 50%-100% for both CFRP and GFRP with the crack arrival. This remarkably large effect is easily detectable and it also allows inferring the position of the delamination front from the pull-out progression at single Z-pin level, as well as whether the crack propagation is stable or not.

6. Conclusions

A method for adding multi-functionality to Z-pinned laminates has been demonstrated at coupon level, through testing of DCB specimens. This approach is based on distributing surface electrodes connecting multiple Z-pins in series/parallel and measuring the through-thickness electrical resistance during progressive delamination growth. The main advantages of the proposed method are that: 1) the Z-pins provide both a mechanical function and a sensing function, enabling delamination detection while increasing the laminate apparent fracture toughness; 2) the TTER variation in the Z-pinned laminate is large enough to allow monitoring the position of the delamination front, as well as the progress of Z-pin pull-out; 3) this sensing approach is suitable for both conductive and non-conductive laminates. However, the applicability of the sensing method to delamination regimes other than pure mode I has still to be demonstrated. The associated characterisation work is ongoing and it will be reported in a separate paper. Demonstrating multi-functionality in mode II is particularly important, since this is the dominating delamination scenario that arises during impact on composite structures. The evidence gathered from the DCB coupons suggests that it is possible to detect Z-pin failure as an abrupt TTER increase. This implies that, in principle, the sensing method can be applied at a relative high mode-mixity (i.e. when approaching mode II), where carbon/BMI Z-pins fail before achieving complete pull-out [26,27]. In addition, Section 4 offers qualitative analysis of the TTER signal, but the Z-pin/electrode contact ER and the Z-pin/laminate contact ER

have to be known in order to give a quantitative analysis. These contact ERs cannot be measured directly and would have to be inferred from micro-scale multi-physics (electro-mechanical) FE models. Thus, the challenges to the quantitative work will be how to accurately estimate the contact ERs. This work is also currently in progress and will be reported in a future publication.

The current embodiment of the multi-functional method leads to a significant weight penalty, i.e. a 10% mass increase for the DCB coupons. However, there is scope for improving the currently manual manufacturing method of the electrodes, which can be in principle 3D-printed on the laminate surfaces. The same holds true for the electrical connections to the external digital multi-meter, which could be arranged in compact and lightweight 3D-printed contact rails.

Finally, the application of the method proposed in this paper to structural elements and sub-components would also require the design of a robust diagnostic system, which must be able to infer the presence an extent of multiple through-thickness delaminations. In principle, fuzzy inference systems or artificial neural networks should be able to perform this task when properly trained in an FE virtual testing framework.

Acknowledgements

The authors would like to acknowledge Rolls-Royce plc for the support of this research through the Composites University Technology Centre (UTC) at the University of Bristol, UK. The authors also wish to thank Dr Julie Etches and Dr Mehdi Yasaee for their help with the development of the experimental set-up.

References

[1] A. Jacob, Carbon fibre and cars – 2013 in review, Reinf. Plast. 58 (2014) 18–19.
[2] G. Marsh, Airbus A350 XWB update, Reinf. Plast. 54 (2010) 20–24.
[3] A.P. Mouritz, B.N. Cox, A mechanistic approach to the properties of stitched laminates, Compos. Part A Appl. Sci. Manuf. 31 (2000) 1–27.
[4] G. Dell'Anno, J.W.G. Treiber, I.K. Partridge, Manufacturing of composite parts reinforced through-thickness by tufting, Robot. Comput. Integr. Manuf. 37 (2015) 262–272.

[5] Y.Q. Wang, A.S.D. Wang, Microstructure/property relationships in three-dimensionally braided fiber composites, Compos. Sci. Technol. 53 (1995) 213–222.
[6] K. Bilisik, Multiaxis 3D woven preform and properties of multiaxis 3D woven and 3D orthogonal woven carbon/epoxy composites, J. Reinf. Plast. Compos. 29 (2009) 1173–1186.
[7] Y. Zhang, L. Yan, M. Miao, Q. Wang, G. Wu, Microstructure and mechanical properties of z-pinned carbon fiber reinforced aluminum alloy composites, Mater. Des. 86 (2015) 872–877.
[8] I.H. Choi, S.M. Ahn, C.H. Yeom, I.H. Hwang, D.S. Lee, Manufacturing of Z-pinned composite laminates, in: Proc. ICCM 17 Conf., Edinburgh, 2009.
[9] S. Kravchenko, O. Kravchenko, M. Wortmann, M. Pietrek, P. Horst, R.B. Pipes, Composite toughness enhancement with interlaminar reinforcement, Compos. Part A Appl. Sci. Manuf. 54 (2013) 98–106.
[10] J.T. Vazquez, B. Castanié, J.-J. Barrau, N. Swiergiel, Multi-level analysis of low-cost Z-pinned composite joints Part 1: Single Z-pin behaviour, Compos. Part A Appl. Sci. Manuf. 42 (2011) 2070–2081.
[11] A.P. Mouritz, T.M. Koh, Re-evaluation of mode I bridging traction modelling for z-pinned laminates based on experimental analysis, Compos. Part B Eng. 56 (2014) 797–807.
[12] D.D.R. Cartié, B.N. Cox, N.A. Fleck, Mechanisms of crack bridging by composite and metallic rods, Compos. Part A Appl. Sci. Manuf. 35 (2004) 1325–1336.
[13] M. Yasaee, J.K. Lander, G. Allegri, S.R. Hallett, Experimental characterisation of mixed mode traction–displacement relationships for a single carbon composite Z-pin, Compos. Sci. Technol. 94 (2014) 123–131.
[14] B. M'membe, S. Gannon, M. Yasaee, S.R. Hallett, I.K. Partridge, Mode II delamination resistance of composites reinforced with inclined Z-pins, Mater. Des. 94 (2016) 565–572.
[15] B.N. Cox, Snubbing effects in the pullout of a fibrous rod from a laminate, Mech. Adv. Mater. Struct. 12 (2005) 85–98.
[16] F. Bianchi, X. Zhang, Predicting mode-II delamination suppression in z-pinned laminates, Compos. Sci. Technol. 72 (2012) 924–932.
[17] G. Allegri, M. Yasaee, I.K. Partridge, S.R. Hallett, A novel model of delamination bridging via Z-pins in composite laminates, Int. J. Solids Struct. 51 (2014) 3314–3332.
[18] M. Meo, F. Achard, M. Grassi, Finite element modelling of bridging micro-mechanics in through-thickness reinforced composite laminates, Compos. Struct. 71 (2005) 383–387.
[19] B. Zhang, G. Allegri, M. Yasaee, S.R. Hallett, Micro-mechanical finite element analysis of Z-pins under mixed-mode loading, Compos. Part A. 78 (2015) 424–435.
[20] F. Pegorin, K. Pingkarawat, A.P. Mouritz, Comparative study of the mode I and mode II delamination fatigue properties of z-pinned aircraft composites, Mater. Des. 65 (2015) 139–146.
[21] I.K. Partridge, D.D.R. Cartié, Delamination resistant laminates by Z-Fiber® pinning: Part I manufacture and fracture performance, Compos. Part A Appl. Sci. Manuf. 36 (2005) 55–64.

[22] K.L. Rugg, B.N. Cox, R. Massabo, Mixed mode delamination of polymer composite laminates reinforced through the thickness by z-fibers, Compos. Part A Appl. Sci. Manuf. 33 (2002) 177–190.
[23] T.M. Koh, S. Feih, A.P. Mouritz, Strengthening mechanics of thin and thick composite T-joints reinforced with z-pins, Compos. Part A Appl. Sci. Manuf. 43 (2012) 1308–1317.
[24] M. Grassi, B. Cox, X. Zhang, Simulation of pin-reinforced single-lap composite joints, Compos. Sci. Technol. 66 (2006) 1623–1638.
[25] J.T. Vazquez, B. Castanié, J.-J. Barrau, N. Swiergiel, Multi-level analysis of low-cost Z-pinned composite joints Part 2: Joint behaviour, Compos. Part A Appl. Sci. Manuf. 42 (2011) 2082–2092.
[26] X. Zhang, L. Hounslow, M. Grassi, Improvement of low-velocity impact and compression-after-impact performance by z-fibre pinning, Compos. Sci. Technol. 66 (2006) 2785–2794.
[27] M. Knaupp, F. Baudach, J. Franck, G. Scharr, Impact and post-impact properties of cfrp laminates reinforced with rectangular z-pins, Compos. Sci. Technol. 87 (2013) 218–223.
[28] F. Bianchi, X. Zhang, A cohesive zone model for predicting delamination suppression in z-pinned laminates, Compos. Sci. Technol. 71 (2011) 1898–1907.
[29] G. Allegri, G. Mohamed, S.R. Hallett, Multi-scale modelling for predicting fracture behaviour in through-thickness reinforced laminates, in: P.P. Camanho, S.R. Hallett (Eds.), Numer. Model. Fail. Adv. Compos. Mater., Woodhead Publishing, 2015: pp. 457–478.
[30] D. Wang, S. Wang, D.D.L. Chung, J.H. Chung, Comparison of the electrical resistance and potential techniques for the self-sensing of damage in carbon fiber polymer-matrix composites, J. Intell. Mater. Syst. Struct. 17 (2006) 853–861.
[31] N.D. Alexopoulos, C. Bartholome, P. Poulin, Z. Marioli-Riga, Structural health monitoring of glass fiber reinforced composites using embedded carbon nanotube (CNT) fibers, Compos. Sci. Technol. 70 (2010) 260–271.
[32] M. Gigliotti, M.C. Lafarie-Frenot, Y. Lin, A. Pugliese, Electro-mechanical fatigue of CFRP laminates for aircraft applications, Compos. Struct. 127 (2015) 436–449.
[33] B. Zhang, G. Allegri, M. Yasaee, S.R. Hallett, I.K. Partridge, On the delamination self-sensing function of Z-pinned composite laminates, Compos. Sci. Technol. 128 (2016) 138–146.
[34] D5528, Standard test method for Mode I interlaminar fracture toughness of unidirectional fiber-reinforced polymer matrix composites, ASTM Stand. (2007).
[35] M.M. Shokrieh, M. Heidari-Rarani, S. Rahimi, Influence of curved delamination front on toughness of multidirectional DCB specimens, Compos. Struct. 94 (2012) 1359–1365.
[36] A.P. Mouritz, B.N. Cox, A mechanistic interpretation of the comparative in-plane mechanical properties of 3D woven, stitched and pinned composites, Compos. Part A Appl. Sci. Manuf. 41 (2010) 709–728.
[37] L. Shen, J. Li, B.M. Liaw, F. Delale, J.H. Chung, Modeling and analysis of the electrical resistance measurement of carbon fiber polymer–matrix composites, Compos. Sci. Technol. 67 (2007) 2513–2520.

Published in Materials & Design, July, 2016
doi: 10.1016/j.matdes.2016.07.035

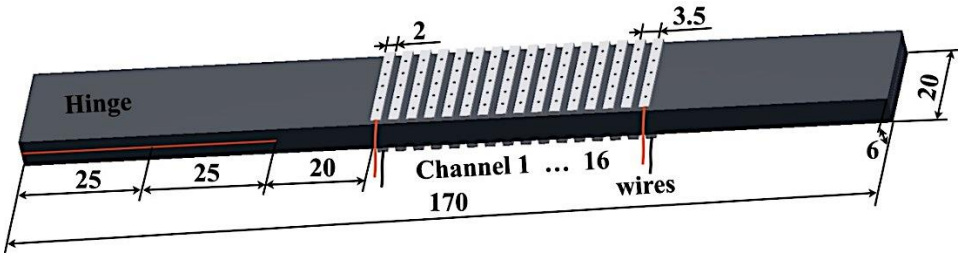

Fig. 1. Schematic diagram of DCB specimens.

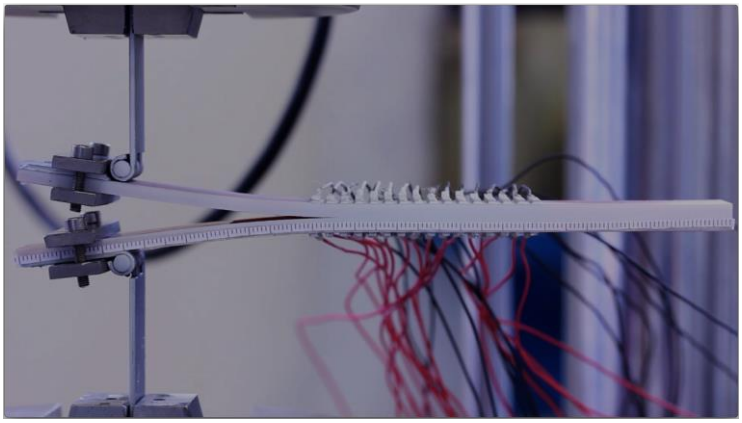

Fig. 2. Snapshot of a DCB coupon under testing.

Published in Materials & Design, July, 2016
doi: 10.1016/j.matdes.2016.07.035

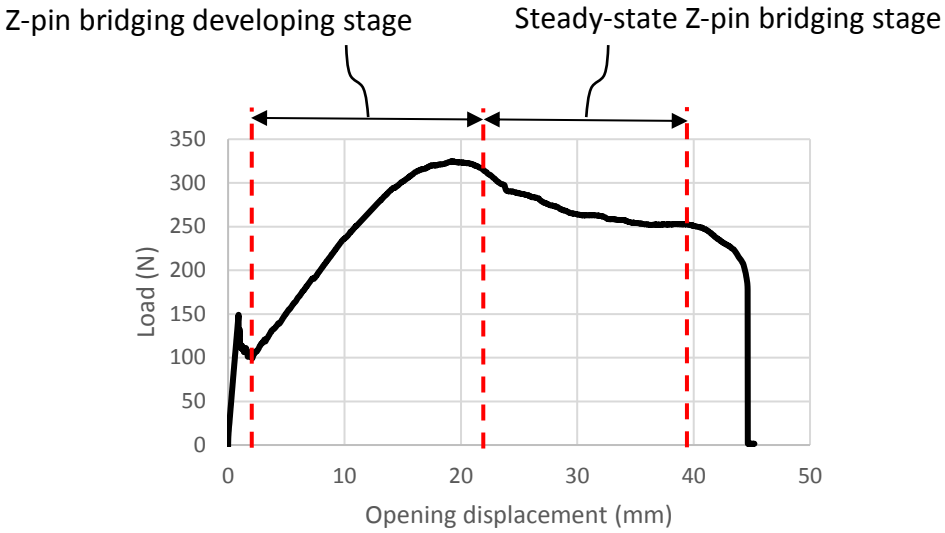

(a)

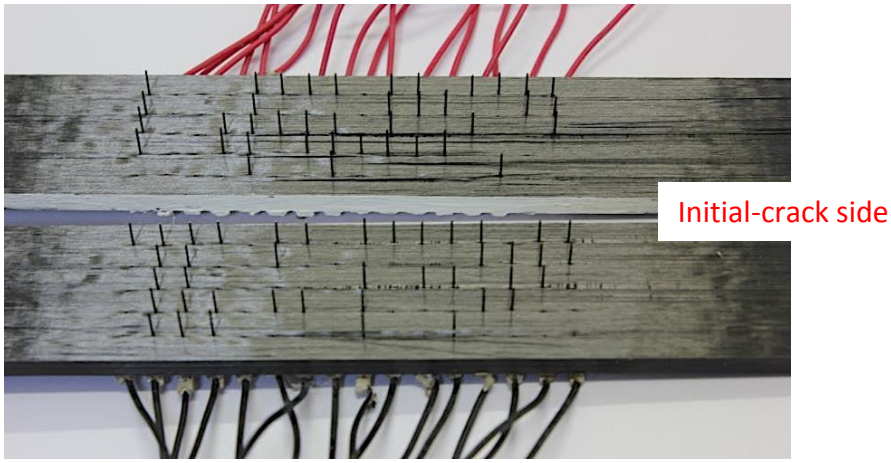

(b)

Fig. 3. (a) Typical load vs. opening displacement curve and (b) opened beams of the Z-pinned CFRP DCB coupon.

Published in Materials & Design, July, 2016
doi: 10.1016/j.matdes.2016.07.035

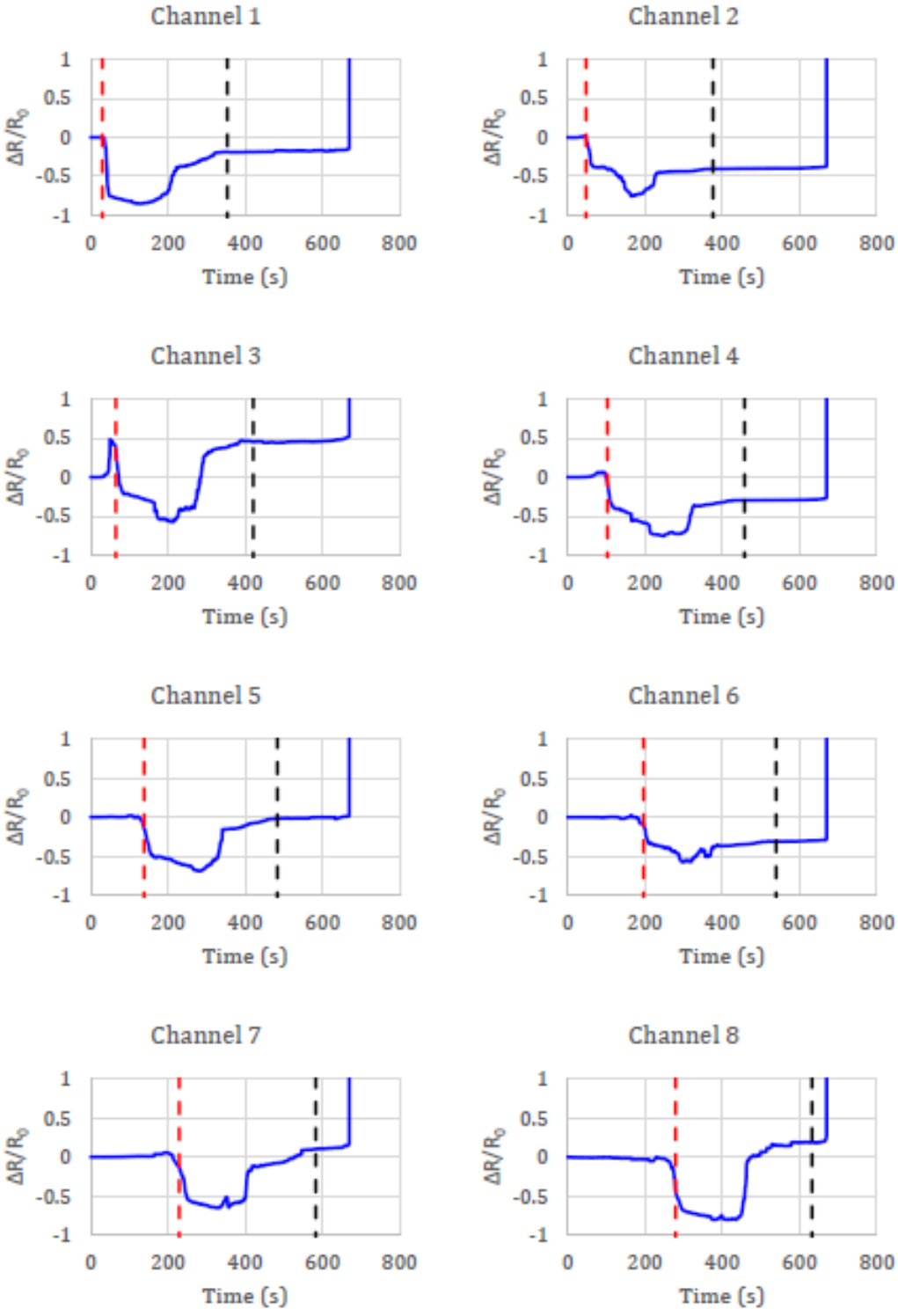

Published in Materials & Design, July, 2016
doi: 10.1016/j.matdes.2016.07.035

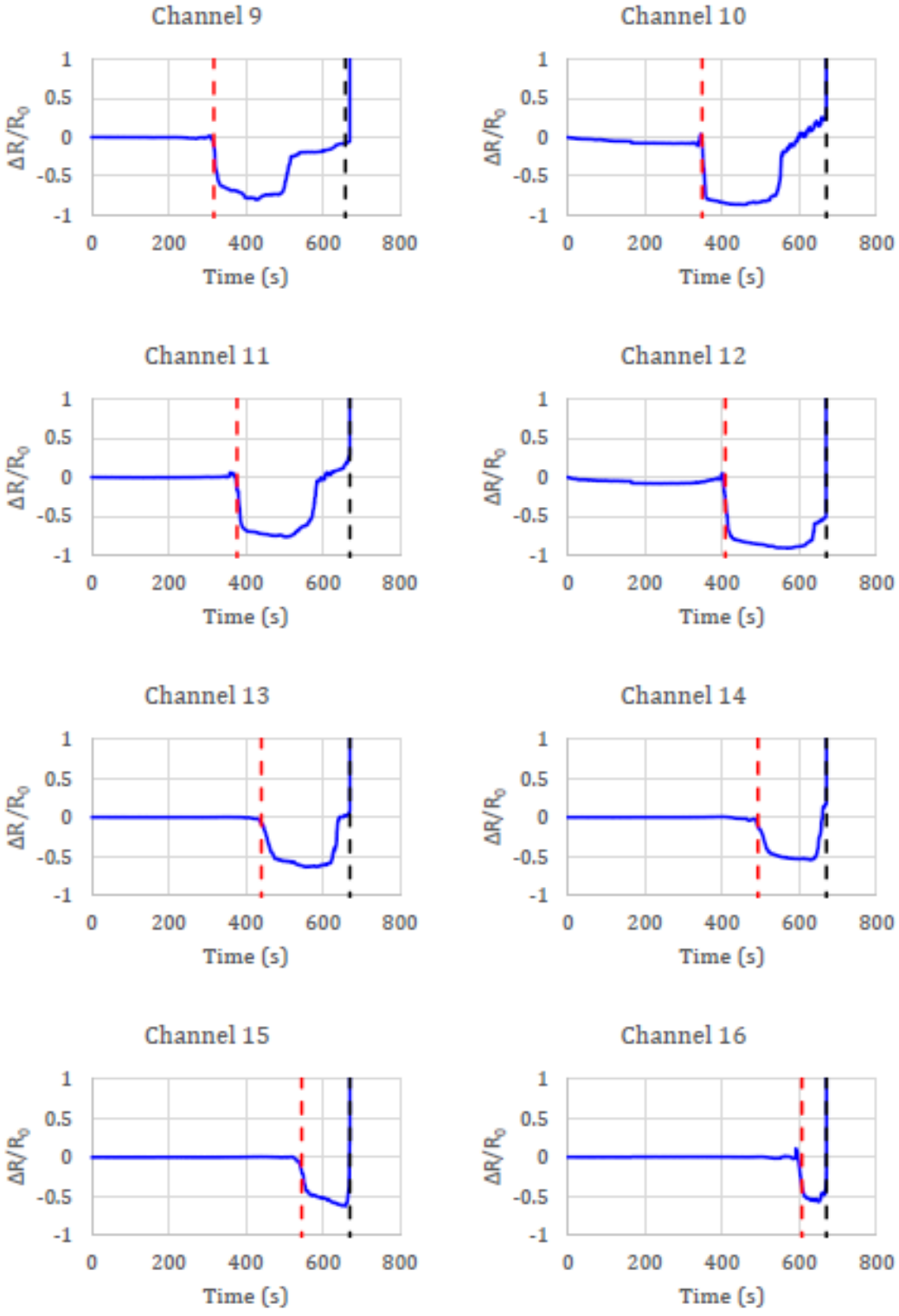

Fig. 4. Typical TTER results of the Z-pinned CFRP DCB coupon; blue curves indicating the fractional TTER change; dashed red lines indicating the time of delamination arrival; dashed black lines indicating the time of complete Z-pin pull-out.

Published in Materials & Design, July, 2016
doi: 10.1016/j.matdes.2016.07.035

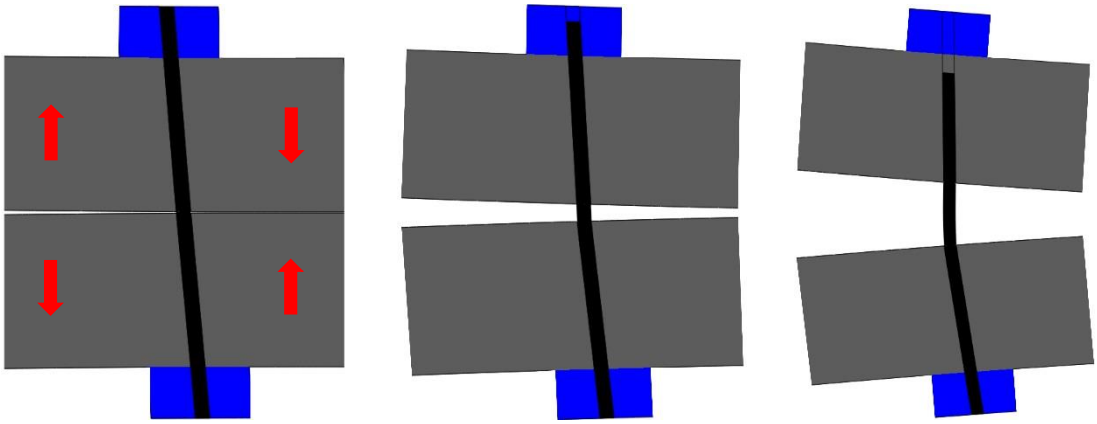

(a) (b) (c)

Fig. 5. Snapshots of (a) crack arrival at a Z-pin, (b) Z-pin pull-out from one electrode and (c) Z-pin pull-out from one laminate beam in the Z-pinned DCB coupon.

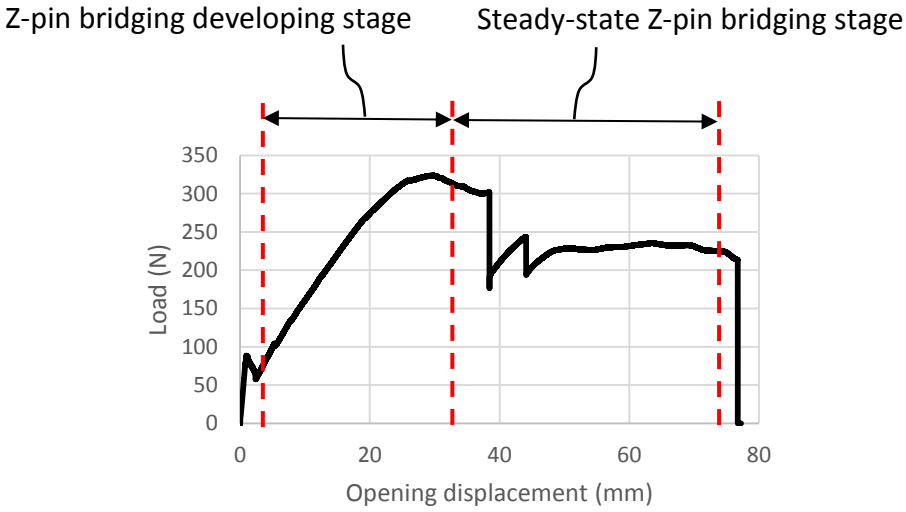

(a)

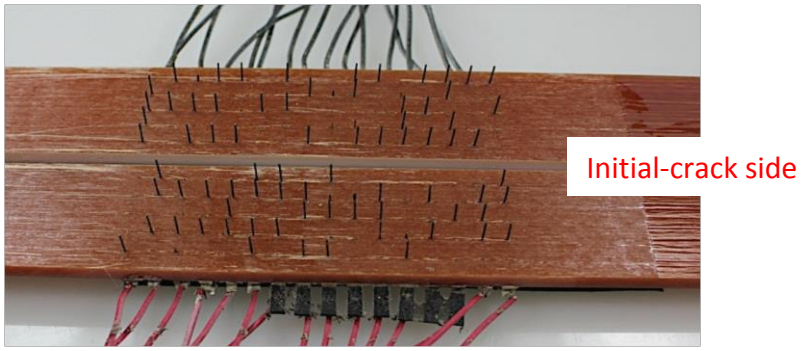

(b)

Fig. 6. (a) Typical load vs. opening displacement curve and (b) opened beams of the Z-pinned GFRP DCB coupon.

Published in Materials & Design, July, 2016
doi: 10.1016/j.matdes.2016.07.035

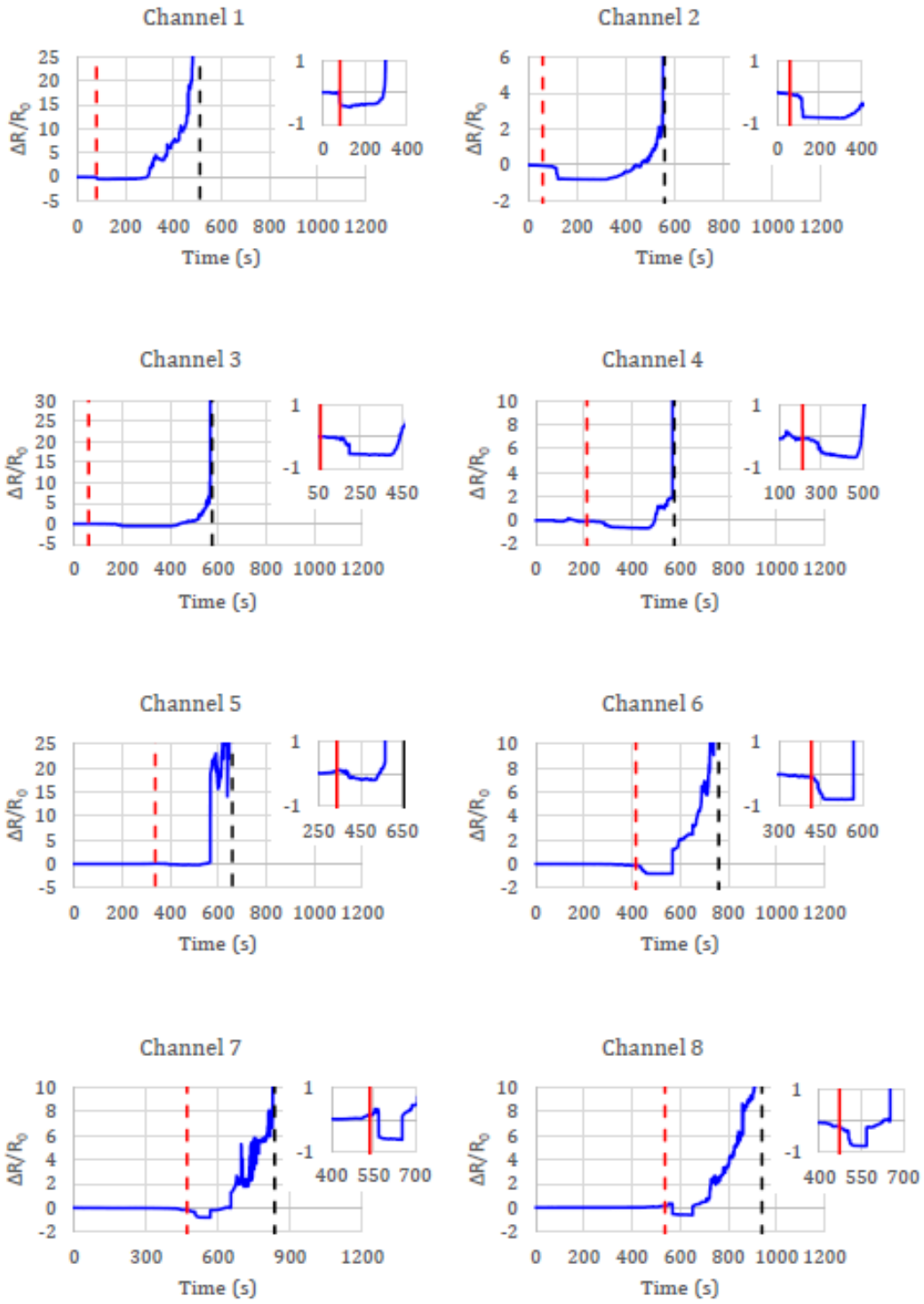

Published in Materials & Design, July, 2016
doi: 10.1016/j.matdes.2016.07.035

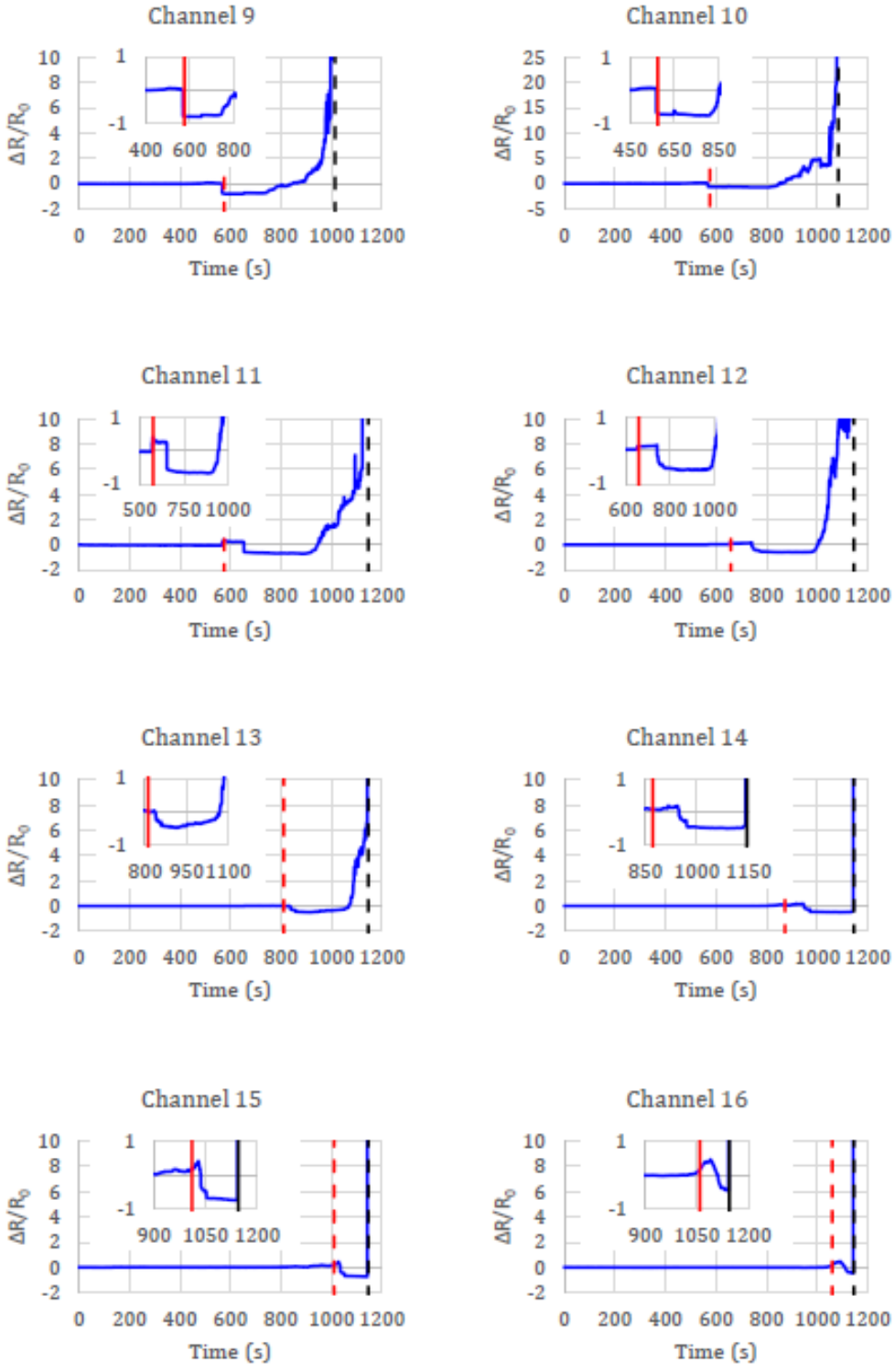

Fig. 7. Typical TTER results of the Z-pinned GFRP DCB coupon; blue lines indicating the fractional TTER change; dashed red lines indicating the time of delamination arrival; dashed black lines indicating the time of complete Z-pin pull-out.